A Composite Modeling Analysis of Impression Creep Testing on Heterogeneous Materials

Model helps predict properties in localized microstructural zones of weld structures

BY M. A. LISIN, I. D. CHOI, D. K. MATLOCK AND D. L. OLSON

ABSTRACT. The high-temperature mechanical properties of weldments containing discrete microstructural zones were investigated with the impression creep test, an indentation creep test that offers the ability to determine the creep properties of minute microstructural zones by monitoring the displacement rate of a cylindrical punch as a function of stress and temperature. The position-dependent creep behavior across the interface of a roll-bonded copper-brass laminate, a material which represents ideal two-component weldments, was evaluated. Impression tests at 450° to 525°C (842° to 947°F) were performed at several locations in the interface region such that the punch deformation field contained varying amounts of each component. A theoretical model for a multicomponent system was developed and was shown to correlate with experimental observations if the deformation field that controlled punch velocity was assumed equal to the punch contact area. The implications of this study with respect to evaluating the localized creep properties within weldments are presented, and the practical usefulness of the impression creep test is discussed.

Introduction

Weldments represent complex heterogeneous materials that contain gradients in microstructure, composition and properties. Predictions of weldment properties frequently depend on the ability to characterize the properties of each individual microstructural zone within the heterogeneous structure of the weld. In addition, prediction of macroscopic properties requires the use of an appropriate composite theory that can accurately describe the interactions between the various microstructural zones.

The heterogeneous structure of welds consists of either fine or coarse gradients. Fine scale gradients result from coring induced compositional changes within individual weld beads (Refs. 1-4). In contrast, coarser microstructural gradients result from bead-to-bead variations in thermal history or due to gradients in both composition and heat from the weld metal to the base metal (Ref. 5).

The effects of microstructural and compositional gradients on mechanical properties of weldments have been considered in several recent publications (Refs. 6-11). All have shown that a complete understanding of the overall properties of welds requires an analysis of position-dependent mechanical properties across the welds.

Several tests have been developed to evaluate localized properties within a weld. These include the use of subsized samples removed from specific local zones (Ref. 12), or the use of samples with microstructures designed to simulate specific zones within the weld. With respect to high-temperature creep properties, the impression creep test (Refs. 13-18) offers the opportunity to evaluate position-dependent properties within a weldment without the need for specialized sample geometries. In the impression creep test the displacement of a cylindrical punch under a constant applied stress is monitored as a function of time. The resistance to deformation is controlled by the material immediately below the punch, and thus, the ability to resolve the properties of local microstructural zones is limited by the punch diameter (Ref. 17). The effects of stress and temperature on measured displacement rates are analyzed and are shown to correlate directly to conventional creep data (Ref. 13).

In two recent studies, impression creep results were correlated directly with microstructural gradients across weldments. Gibbs, *et al.* (Ref. 19), in his study of the creep behavior across austenitic to ferritic steel dissimilar metal weldments, showed that the minimum in creep resistance occurs in a zone adjacent to the fusion line where creep cracking has been observed in service. Wang, *et al.* (Ref. 20) evaluated bead-to-bead variations in the creep properties across a multipass ASTM-A36 steel weld. Specifically, the creep properties on a traverse from the cast microstructure of the last bead, through the reheat-affected zone of the next-to-last bead, and into the aged microstructure of the next-to-last bead were measured. The microstructures associated with this traverse are illustrated in Fig. 1, and the corresponding impression creep velocity data are shown in Fig. 2. The reheat-affected zone of the next-to-last bead consists of fine equiaxed ferrite, while the solidified zones of both beads consist of columnar grains of fine acicular ferrite surrounded by either elongated or equiaxed proeutectoid ferrite. The acicular ferrite zone in the next-to-last

KEY WORDS

Composite Modeling
Impression Creep
Impression Tests
Creep Testing
Heterogeneous Materials
Cu-Brass Laminates
Laminate Composites
Microstructural Zone
Punch Velocities
Activation Energies

M. A. LISIN is with San Diego Gas and Electric, San Diego, Calif. I. D. CHOI, D. K. Matlock and D. L. Olson are with the Center for Welding and Joining Research, Colorado School of Mines, Golden, Colo.

Paper presented at the 70th Annual AWS Meeting, held April 2-7, 1989, in Washington, D.C.

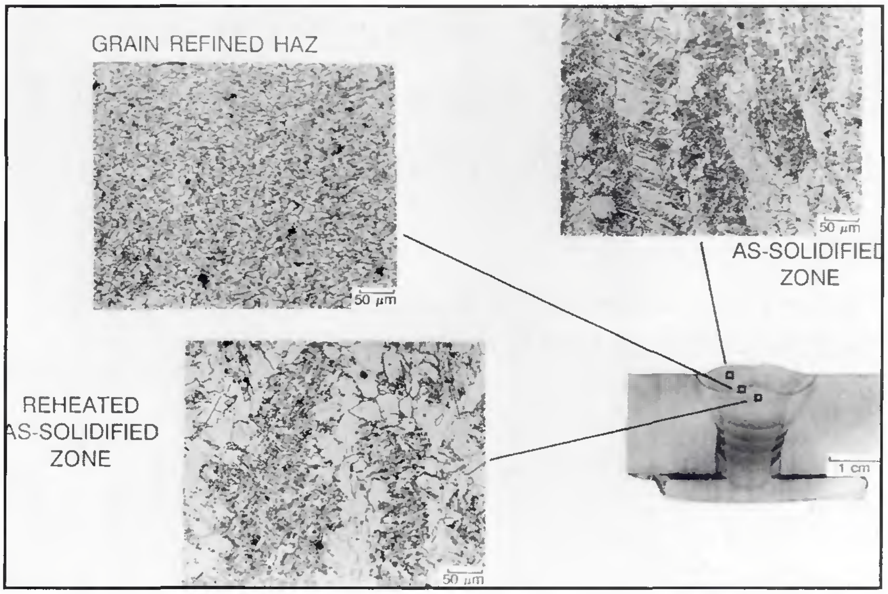

Fig. 1—Microstructural zones existing within a multipass SMAW A36 low-carbon steel weldment. Light photomicrograph, nital etch. From Ref. 20.

bead appears to have coarsened due to aging. The minimum in creep resistance, as evidenced by a maximum in impression creep punch velocity, occurs in the fine-grained, reheat-affected zone. The observation of a decrease in creep resistance with grain refinement is consistent with general creep theory (Ref. 21). These results on ASTM A36 indicate that the variations in creep behavior across the multipass weldment mirror the variations in microstructure.

To date, impression creep tests on weldments have been unable to determine properties within a single microstructural zone. This inability stems from the fact that the indenter plastic zone contains multiple components. In addition, continuous gradients from one zone to the next make the delineation of individual components difficult. In order to extend the impression creep test to complete analyses of weld metal with continuous microstructural gradients; an appropriate composite theory is required. In this paper, the basics of such a theory are developed and predictions are compared to impression creep data.

An ideal material for study should consist of microstructural gradients with well-defined interfaces between microstructural zones. Furthermore, each zone should be larger than the punch diameter so that the impression creep properties of the individual zones can be determined. To simplify the analysis, a two-component roll-bonded laminate composite was chosen. In the composite, impression creep data were obtained in each base metal and as a function of position across the diffusion-bonded interface.

Experimental Procedure

A roll-bonded laminate composite was fabricated from copper Alloys C11000 (commercially pure copper) and C26000 (cartridge brass, nominally 70% Cu and 30% Zn). The composition and initial plate thickness of each alloy are shown in Table 1. Two 102- × 150-mm (4- × 6-in.) plates, one of each alloy, were encased in a stainless steel canister attached to an active vacuum system and preheated to 820°C (1508°F). The canister was hot rolled on a laboratory rolling mill and the thickness was reduced 20% in multiple passes. Metallographic analysis and room-temperature mechanical testing verified that a complete bond was obtained (Ref. 22). In addition, prior to creep testing, the composite was annealed at 625°C (1157°F) for 4 h.

Impression creep tests were performed with the test system developed by Gibbs (Refs. 17,19). A 1-mm (0.040-in.) diameter molybdenum punch was used. Creep data for the copper-brass system were obtained at temperatures between 450° and 525°C and stresses between 90 and 117 MPa (13 and 17 ksi).

The microstructure of the composite prior to testing and the deformed zones below the punch were analyzed with standard light metallographic techniques. The copper-brass composite was etched in a solution of 5g $K_2Cr_2O_7$, 20 mL H_2SO_4, 5 mL HCl and 250mL H_2O. Chemical analysis across the laminate composite was obtained with a JEOL JXA-840 scanning microanalyzer.

Results

Two sets of experimental impression creep data were obtained to provide in-

Table 1—EDS Analysis of the Test Material Compositions (wt-%)

	Cu	Ni	Zn	Co	Fe	Mn
C11000 (12.7mm)	99.9	0.01	0.05	0.01	0.02	0.01
C26000 (12.7mm)	69.2	—	30.6	0.01	0.05	0.14

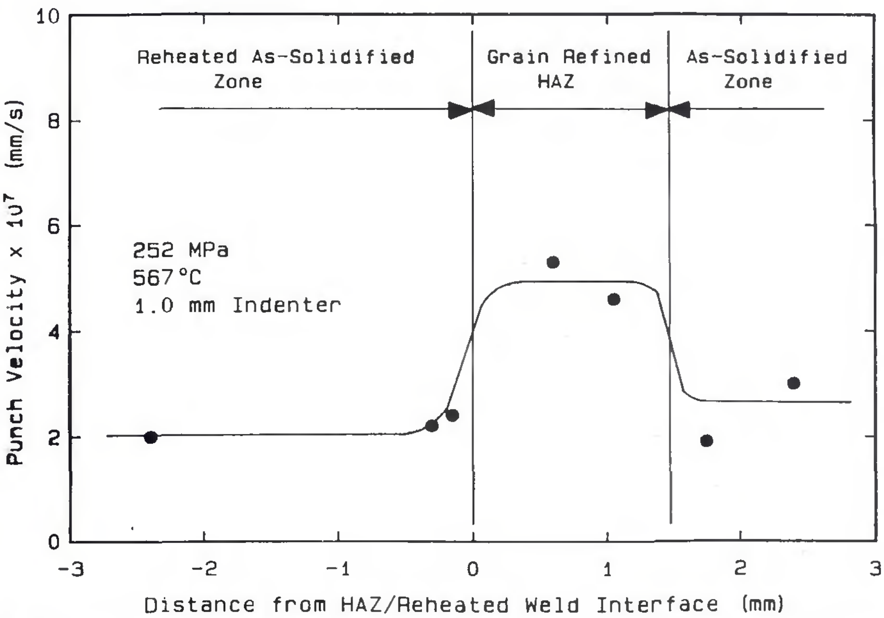

Fig. 2—Steady-state impression creep punch velocity as a function of position within the multipass SMAW A36 low-carbon steel weldment shown in Fig. 1. From Ref. 20.

Fig. 3 — Light micrographs. A — The copper component; B — the interface; C — the brass component in the copper-brass laminate.

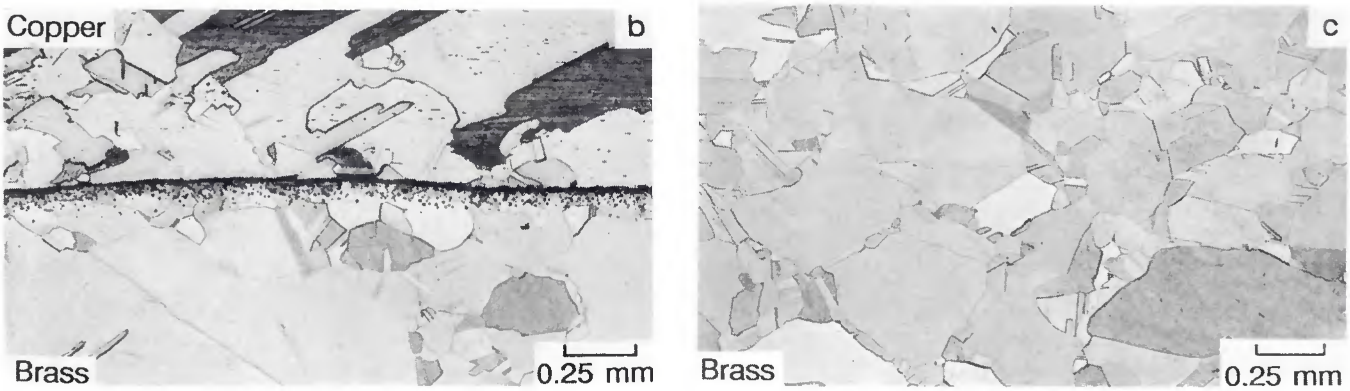

put to the composite model analysis, which follows in the Discussion section. First, impression creep properties of each base material in the composite were determined. Then, the effect of position with respect to the interface was evaluated. Light micrographs of the base materials and interface are shown in Fig. 3. Both base metals consist of a duplex grain structure in the annealed condition. The interface shows a complete bond and the base metal grain structures are constant up to the interface. The zinc and copper compositions adjacent to the interface were measured with energy dispersive spectroscopy (EDS) techniques, and the results are shown in composition profiles in Fig. 4. Figure 4 shows that the gradient in composition occurs entirely within 0.1 mm of the interface. The dimension represents 10% of the punch diameter. Consequently, tests in the interface region represented primarily the properties of the two components, with only a small contribution to punch velocity from the continuous compositional gradient region.

Impression Creep of Base Metal

Typical impression creep curves for the copper and brass base metals at 475°C and a punch stress of 117MPa (17 ksi) are shown in Fig. 5. Both curves show a region of transient creep, in which the punch velocity (*i.e.*, the slope of the displacement-time curve) decreases with displacement, and a region of steady-state creep where the velocity is constant, independent of displacement. Steady-state punch velocities were taken as the average punch velocity between 12 and 36 h. Also note that the steady-state punch velocity of the brass is approximately 3.9 times that of the copper. The creep rates of the two constituents are different enough that the influence of one component on the creep rate of a two-component composite should be easily detected, and yet the two creep rates are similar enough that they can both be measured accurately under identical stress and temperature conditions. It should be noted the microstructures of the as-tested samples revealed microstructural changes below the punch: recrystallization in brass and grain growth in copper (Ref. 22). However, a systematic microstructural examination showed that all changes in microstructure developed within the first 12 h, and microstructures were stable (Ref. 22) for times greater than 12 h. Therefore, the measured steady-state creep rates reflected a constant mi-

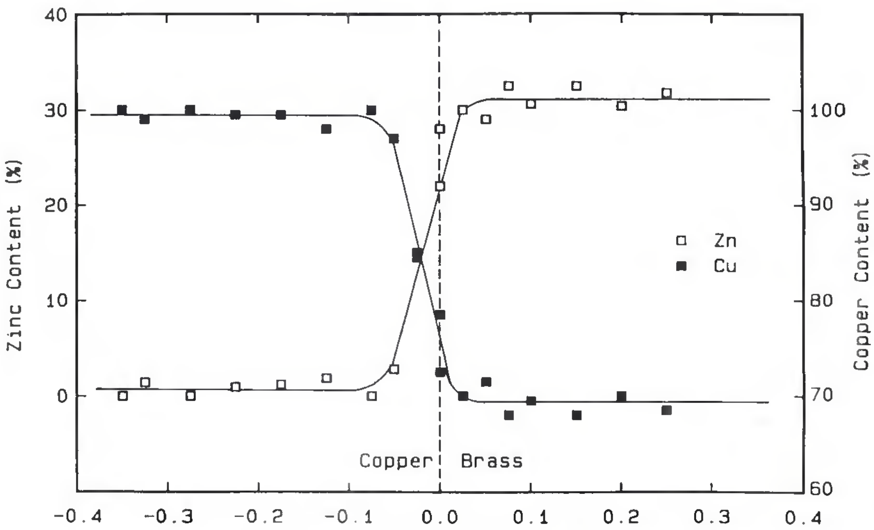

Fig. 4 — The effect of position on the zinc and copper compositions (EDS analysis) in the interfacial region of the copper-brass laminate.

Table 2—Creep Activation Energies and Stress Exponents for Copper and Brass Alloy C26000 Obtained with Conventional Creep Samples

Material	Temperature °C	Activation Energy kcal/mole	Interpreted Mechanism	Stress Exponent	Reference
Copper	above 610	48.0	—	4.8	23
	405 to 610	28.0	—	4.8	23
	450 to 530	32.8	—	5	24
	413	27.5	—	4.8	25
	above 510	42	—	5.0	27
	—	49.6	(bulk diffusion)	—	26
	—	24.8	(boundary diffusion)	—	26
	500	20.2	(boundary diffusion)	—	31
Brass Alloy 260	413	—	—	4.5	28
	550 to 700	31	—	5	29
	—	30	—	—	30
	500	12.5	(boundary diffusion)	—	31
	—	—	—	4.5	32
	500	41.9	(bulk diffusion)		33

crostructural condition.

The effects of stress and temperature on punch velocities were analyzed according to the following equation:

$$v_p = B\sigma^n \exp(-Q/RT) \qquad (1)$$

where v_p is the punch velocity, σ is the true stress, n is the stress exponent, Q is apparent activation energy for impression creep, B is a constant, and R and T have their usual meanings. Previous studies (Ref. 13) have shown that v_p, n and Q obtained from impression creep data relate directly to conventional creep data.

The effects of stress at constant temperatures on steady-state impression creep velocities are shown in Figs. 6 and 7 for copper and brass, respectively. Correspondingly, the effects of temperature at constant stresses are shown in Figs. 8 and 9. The linear relationships shown in Figs. 6 to 9 indicate that Equation 1 is applicable to both copper and brass for the test conditions of this study.

From the slopes of Figs. 6 and 7, the stress exponents, n, were obtained for each system. An average stress exponent of 4.0 was calculated for both materials. The maximum deviation in n was obtained in the brass system with measured values between 3.9 and 4.05.

The plots of punch velocity versus inverse absolute temperature in Figs. 8 and 9 yield values of the apparent activation energies for impression creep. The slopes are approximately equal at each stress level, suggesting that the activation energies remain constant within the stress range investigated. Furthermore, the fact that data plot linearly and parallel at each stress level indicates that the same creep mechanism or mechanisms dominate over the entire stress and temperature ranges investigated. Average activation energy for copper is 17.4 kcal/mole, and for brass is 25.2 kcal/mole. Maximum deviation in the individual activation energies for both materials at each stress level was less than 7% of the average value.

The significance of the measured n and Q values for impression creep in each system can be evaluated by comparing these results to published Q and n values, summarized in Table 2, obtained on conventional creep samples. The measured stress exponent of 4.0, although slightly lower, is in reasonable agreement with the published values which range between 4.5 and 5.0.

The published creep activation energies for brass and copper vary significantly. A

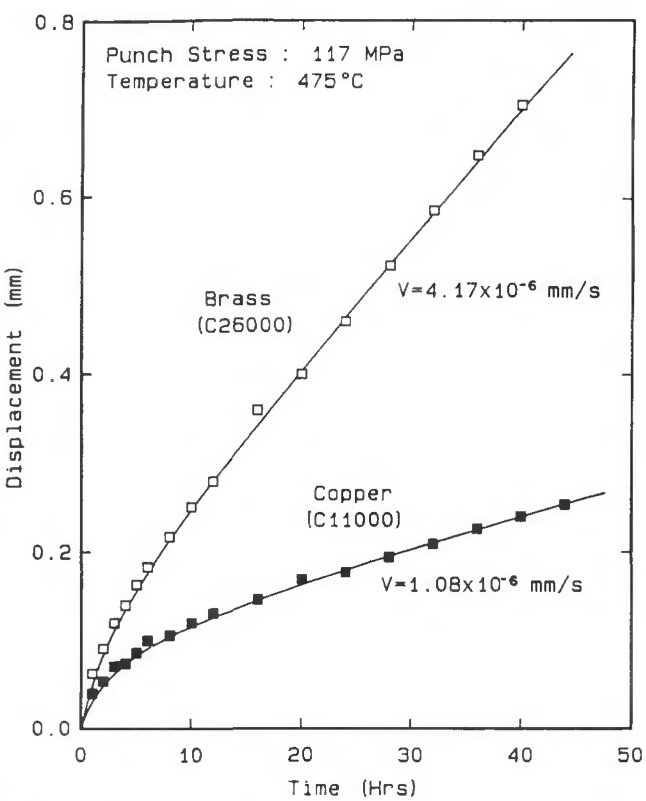

Fig. 5 — Impression creep curves for the unlaminated copper and brass plate materials tested at 475°C and 117 MPa.

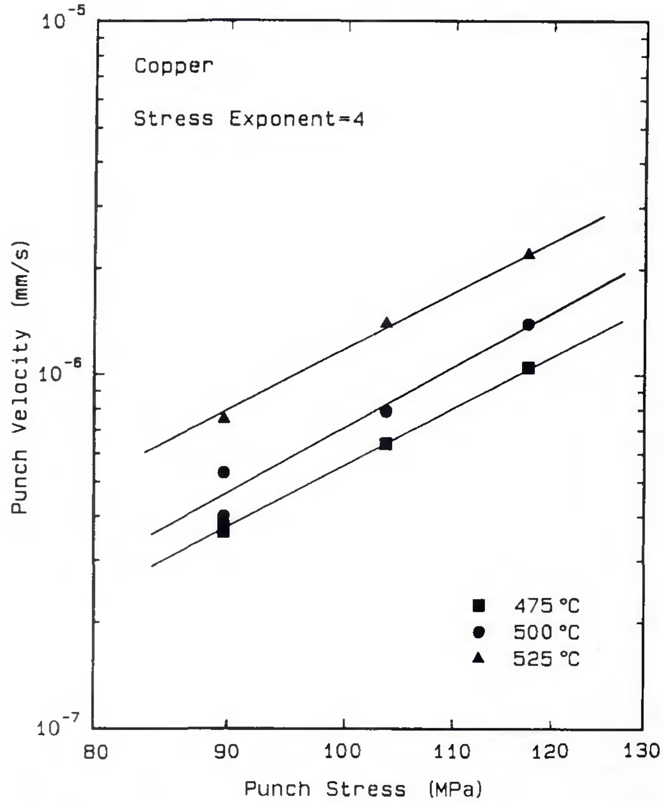

Fig. 6 — The effect of stress on the steady-state impression punch velocity for copper at three test temperatures. The slope is equal to the stress exponent in Equation 1.

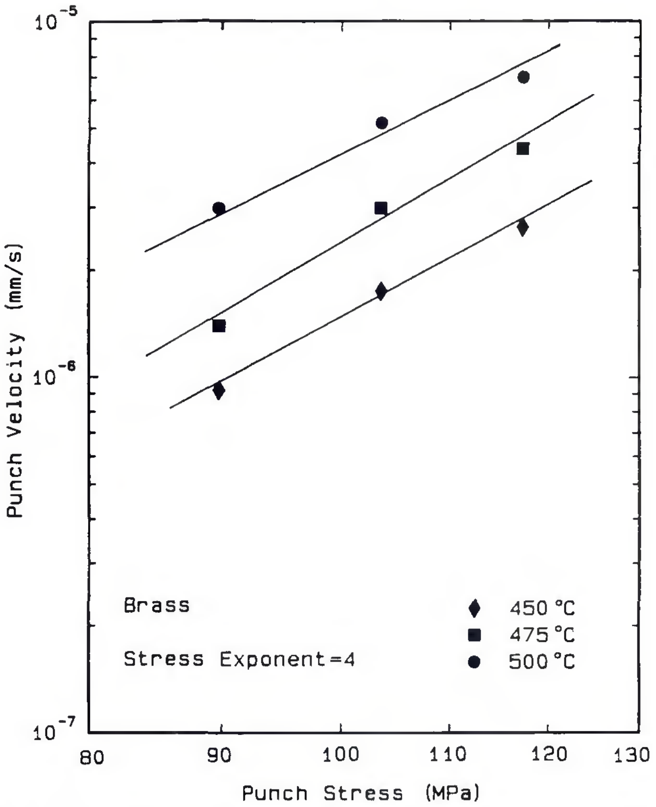

Fig. 7 — The effect of stress on the steady-state impression punch velocity for brass at three test temperatures. The slope is equal to the stress exponent in Equation 1.

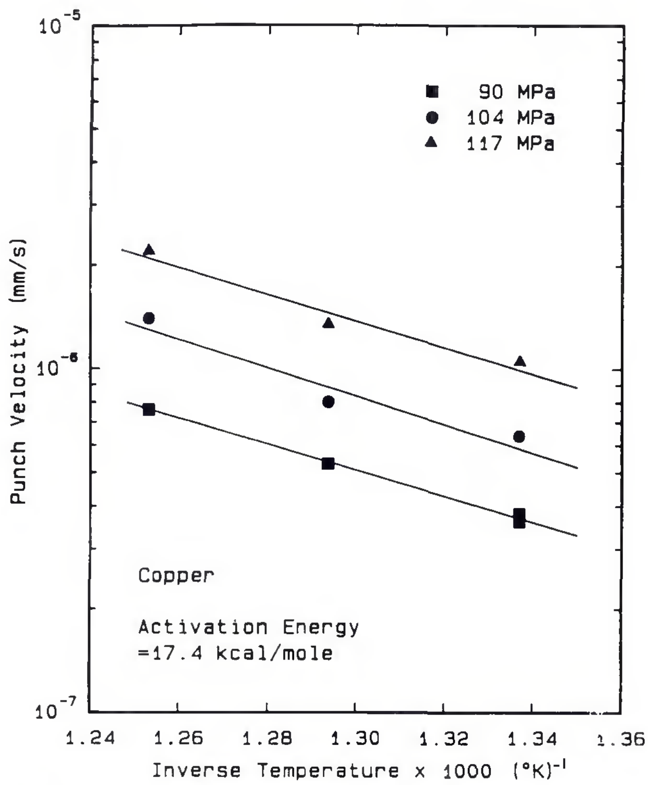

Fig. 8 — The effect of temperature on the steady-state impression punch velocity for copper at three stresses. The slope is equal to Q/R in Equation 1.

comparison with the data in Table 2, shows that for both systems the apparent activation energies for impression creep compare with the lower values for conventional creep.

With the measured n and Q values for impression creep of copper and brass, the preexponential constants in Equation 1 were determined, and the following unified velocity equations were developed (with v in mm/s and σ in MPa).

$$v_p(\text{copper}) = 7.1 \times 10^{-10}\sigma^4 \exp\left(\frac{-17.4 \text{ kcal/mole}}{RT}\right) \quad (2)$$

$$v_p(\text{brass}) = 5.8 \times 10^{-7}\sigma^4 \exp\left(\frac{-25.2 \text{ kcal/mole}}{RT}\right) \quad (3)$$

These equations were shown to adequately describe all of the impression creep data of this study.

Impression Creep of Laminate Composites

Punch velocity data at positions that traverse the interface region are plotted as a function of location with respect to the interface in Fig. 10. Each data point in this figure indicates the position of the punch centerline with respect to the interface. All tests plotted in this figure were performed at a punch stress of 104 MPa (15 ksi) and a test temperature of 475°C (855°F). Also indicated in this figure is the diameter of the indenter. Note that the indenter diameter is much larger than the symbols used to plot the data. Thus, a data point located 0.5 mm (0.020 in.) from the interface indicates that the punch is entirely within one component, and that the punch wall is tangent or immediately adjacent to the interface. Two predictions, based on a theory developed below for impression creep within a multicomponent system, are also shown.

Figure 10 shows that in a test in which the punch was located entirely within the copper but immediately adjacent to the interface, the punch velocity is approximately equal to the average punch velocity within the copper away from the interface. This indicates that the adjacent brass material had no effect on the punch velocity at this location. This same observation holds true for tests conducted in the brass. Consider the data point located at −0.62 mm. In this case, the punch wall is only 0.12 mm (0.005 in.) from the interface, yet the punch velocity is within the scatter for the average punch velocity within the brass. These observations show that only the material immediately below the punch controls the punch velocity.

Discussion

The effect of punch position with respect to the interface on the impression creep velocities can be evaluated following the composite modeling approach introduced by Gibbs (Ref. 17). This analysis, based on an isostrain composite, is summarized below and is a uniform strain approximation of the deformation behavior within a nonuniform deformation zone.

The applied load in impression creep is supported by the effective volume of material that is deformed below the punch. If this volume includes two components, then the applied load, F_p, is:

$$F_p = F_1 + F_2 \quad (4)$$

where F_1 and F_2 are the loads supported by the two components.

The average applied stress within the deformation zone, σ_p, is:

$$\sigma_p = \frac{F_p}{\alpha A_p} \quad (5)$$

where A_p is the actual punch area and α is a parameter ($\alpha \geq 1$) that defines the size of the deformation zone. Correspondingly, the stresses in each zone are:

$$\sigma_1 = \frac{F_1}{A_1} \quad (6)$$

$$\sigma_2 = \frac{F_2}{A_2} \quad (7)$$

where:

$$A_1 + A_2 = \alpha A_p \quad (8)$$

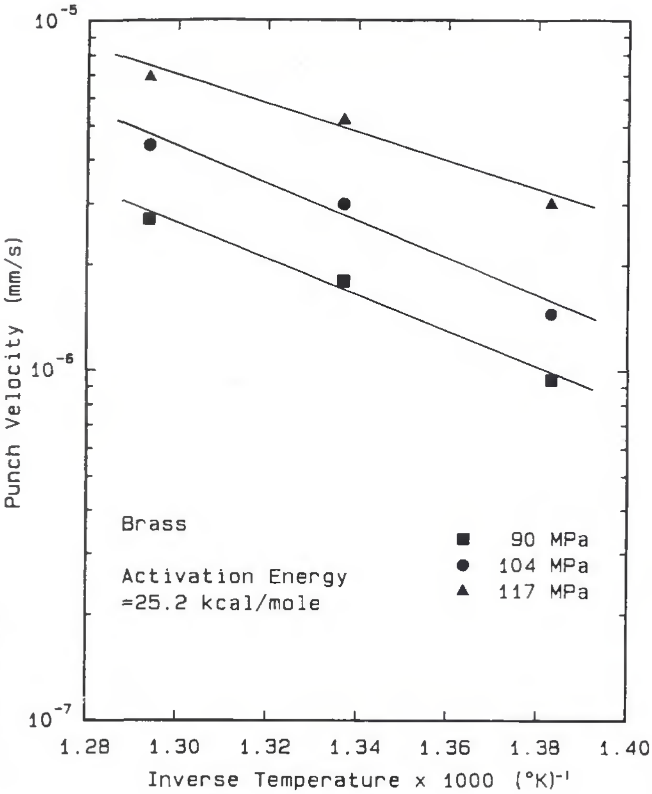

Fig. 9 — The effect of temperature on the steady-state impression punch velocity for brass at three stresses. The slope is equal to Q/R in Equation 1.

and A_1 and A_2 are the deformation areas in each component. The area fraction of each component are:

$$X_1 = \frac{A_1}{\alpha A_p} \tag{9}$$

$$X_2 = \frac{A_2}{\alpha A_p} \tag{10}$$

Combining Equations 6 to 10 with Equation 4 yields the rule of mixtures expression for stress:

$$\sigma_p = X_1\sigma_1 + X_2\sigma_2 \tag{11}$$

For this system, the average punch velocity, v_p, is equivalent to the punch velocities within each zone, such that:

$$v_p = v_1 = v_2 \tag{12}$$

At a constant temperature (with $K = B\exp(-Q_i/RT)$):

$$v_1 = K_1\sigma_1^{n_1} \tag{13}$$

$$v_2 = K_2\sigma_2^{n_2} \tag{14}$$

with $n_1 = n_2$, as is the case for the copper and brass of this study, combining Equations 12, 13, and 14 with Equation 11 yields:

$$\sigma_p = v_p^{1/n}\left\{\frac{X_1}{K_1^{1/n}} + \frac{X_2}{K_2^{1/n}}\right\} \tag{15}$$

Solving Equation 15 for v_p results in the following expression, which can be compared to the experimental data:

$$v_p = \left[\frac{\sigma_p}{\frac{X_1}{K_1^{1/n}} + \frac{X_2}{K_2^{1/n}}}\right]^n \tag{16}$$

To utilize Equation 16, two conditions must be specified: the position of the punch with respect to the interface and the effective size of the deformation zone (i.e. α in Equation 5). Previous analyses, which have included metallographic observations of surface deformation adjacent to the punch (Refs. 14, 17) and slip line field calculations, have indicated that the diameter of the deformation zone may be as much as three times the punch diameter. A deformation zone diameter three times the punch diameter is described by an α (in Equation 5) of 9.

To evaluate the data shown in Fig. 10, two predictions of the position-dependent impression punch velocity were made; one with an α of 1, a calculation that assumes the zone immediately below the punch controls the punch velocity, and one with an α of 9. The significance of the choice of α on the calculated component area fractions that correspond to a specific punch position is illustrated in the following example calculation. With the interface 0.4 mm (0.016 in.) from the centerline of a 1-mm (0.040-in.) diameter punch, the area fraction of the minority constituent is only 0.052 for $\alpha = 1$, but is 0.33 for $\alpha = 9$.

The predicted punch velocities for α values of 1 and 9 are plotted in Fig. 10 along with the experimental data. Both calculations show a continuous transition in the impression creep behavior across the interface. The continuous transition extends to further distances from the interface with an increase in α. A comparison of the experimental data with the theoretical predictions in Fig. 10 shows that there is excellent agreement for the case of $\alpha = 1$. This correlation implies that the material immediately below the punch primarily controls the observed impression punch velocity.

In addition to the copper and brass data in which the creep rates of the base materials differed by less than one order of

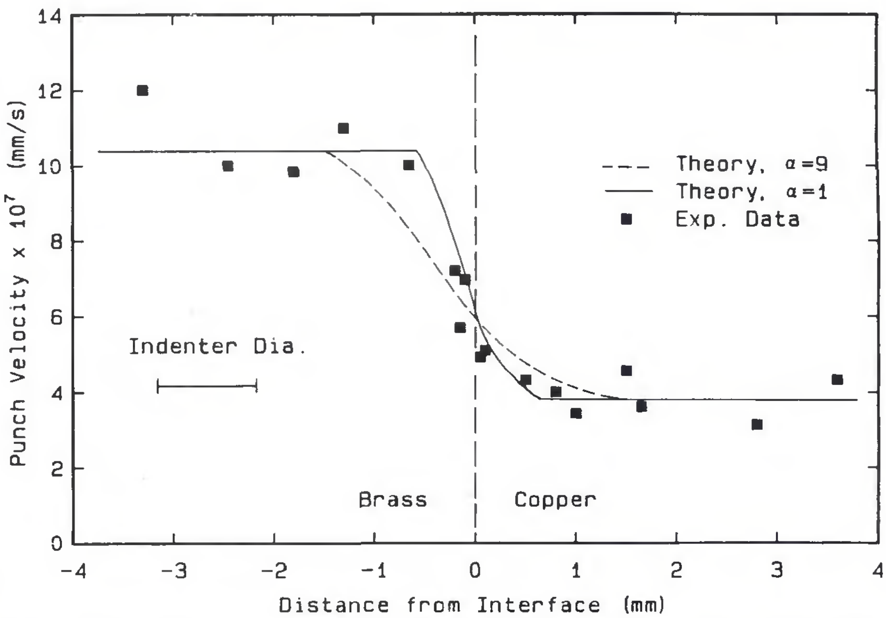

Fig. 10 — Punch velocity in the interface region of the copper-brass laminate. The horizontal position of the data indicates the location of the punch centerline with respect to the interface. The punch stress was 104 MPa, and the test temperature was 475°C. Predictions of the composite model for two assumed deformation zone sizes are shown.

magnitude, the material immediately below the punch controlled punch rates in a nickel-copper laminate composite, where the base metal impression punch velocities differed by greater than two orders of magnitude (Ref. 22). The observations in both the copper-brass and copper-nickel systems are significant with respect to impression creep testing within weldments containing fine microstructural gradients. The data provide an upper limit to punch diameter when attempting to characterize the creep properties of minute microstructural zones. As long as the punch fits entirely within the microstructural zone of interest, the measured creep properties will not significantly be affected by the adjacent microstructural zones.

A composite modeling approach has been presented for the analysis of impression creep data in a simple two-component system. The theoretical predictions were shown to correlate with experimental observations where the deformation zone that controls punch was assumed equal to the punch diameter. In more complex systems, such as weldments in which the deformation zone may contain more than two discrete microstructural zones or a continuous microstructural gradient, it should be possible to predict localized creep properties from impression creep measurements by using a direct analog of the analysis presented in this paper. An example analysis of this approach is presented elsewhere (Ref. 22).

The impression creep test provides a simple method to evaluate the local creep properties of materials. Several potential industrial applications exist:

1) The existence and location of zones with low creep strengths within a weldment can be determined by a direct comparison of punch velocities. This information can guide welding procedure and material selection.

2) Changes in punch velocity and consequently creep resistance can be determined as a function of time. This allows a direct comparison of the service behaviors of candidate materials, welding procedures, heat treatments, etc. The effects of time-dependent microstructural changes (*e.g.,* carbide formation, grain growth and decarburization) can be evaluated.

3) Punch velocity data can be used in an activation energy analysis. The resulting activation energy can be used in a Larson-Miller type of analysis for the prediction of residual life.

Conclusions

1) Impression creep data have been obtained for copper Alloys C11000 and C26000 (brass). Both materials display a stress exponent equal to 4.0. Activation energies of 17.4 kcal/mol for copper and 25.2 kcal/mol for brass have been determined. These values compare favorably with published values obtained from conventional creep tests.

2) Copper-brass laminates have been successfully fabricated by roll bonding. The materials have provided ideal systems for modeling of microstructural gradients.

3) Based on the predictions of a two-component composite model, the impression creep punch velocity appears to be influenced primarily by material immediately under the punch. This provides an upper limit to punch diameter when performing impression creep tests within microstructural gradients such as weldments.

Acknowledgments

The authors appreciate and acknowledge the research support of the Office of Basic Science of the U.S. Dept. of Energy. Also, the assistance of Mr. Shing-Hoa Wang with the work on A36 steel cited in the Introduction is appreciated.

References

1. Korzh, T. V., Okenko, A. P., Chernyshova, T. A., and Mirochnik, V. L. 1985. Micromechanical and structural heterogeneity of weld metal of low-alloy steel. *Welding Production* (2): 37.

2. Savage, W. F., Nippes, E. F., and Miller, T. W. 1976. Microsegregation in 70Cu-30Ni weld metal. *Welding Journal* 55 (6): 165-s.

3. Sterenbogen, Y.A., Demchenko, V. F., and Abdulakh, V. M. 1977. Research into the process of development of chemical heterogeneity during the solidification of weld metal. *Automatic Welding* 30 (2): 3.

4. Savage, W. F., Lundin, C. D., and Aronson, A. H. 1965. Weld metal solidification mechanics. *Welding Journal* 44 (4): 175-s.

5. Serrano, O. V. 1979. A comparison of as-welded and stress relieved 2¼ Cr-1 Mo steel electroslag weldments. M.S. Thesis T-2272, Colorado School of Mines, Golden, Colo.

6. Berry, G. 1988. Compositional gradient effects on stress corrosion cracking behavior of weld metal. M.S. Thesis T-3640, Colorado School of Mines, Golden, Colo.

7. Meitzner, C. F. 1975. Stress relief cracking. *WRC Bulletin No. 211.*

8. Kearns, W. H. ed. 1982. *Welding Handbook.* Vol. 14, 7th ed. American Welding Society, Miami, Fla., p. 48.

9. Fairchild, D. P. 1987. Local brittle zones in structural steel welds. Presented at the *International Symposium on Welding Metallurgy of Structural Steels.* Denver, Colo.

10. Sterenbogen, Y. A. 1980. Solidification of the weld pool and the effect of its composition on the chemical heterogeneity and susceptibility of welds to solidification cracking. *Proceedings of International Conference on Weld Pool Chemistry and Metallurgy.* The Welding Institute, Cambridge, England, p. 31.

11. Katayama, S., Fujimoto, T., and Matsunawa, A. 1985. Correlation among solidification process, microstructure, microsegregation and solidification cracking susceptibility in stainless steel weld metals. *Trans. JWRI* 14 (1): 123.

12. Cavdenas, C., Pense, A. W., and Stout, R. D. 1979. The fracture toughness of a high-strength Ni-Cr-Mo alloy steel weldment. *Applications of Materials for Pressure Vessels and Piping,* ed. George V. Smith, ASME, New York, N.Y., p. 137.

13. Chu, S. N. G., and Li, J. C. M. 1977. Impression creep, a new creep test. *J. Mat. Sci.* 12: 2200.

14. Chu, S. N. G., and Li, J. C. M. 1979. Impression creep of β-tin single crystals. *Mat. Sci. and Eng.* 39: 1.

15. Chu, S. N. G., and Li, J. C. M. 1980. Computer simulation of impression creep by finite element method. *J. Mat. Sci. 15:* 2733.

16. Yu, E. C., and Li, J. C. M. 1977. Impression creep of LiF single crystals. *Phil. Mag.* 36 (4): 811.

17. Gibbs, W. S. 1983. High-temperature impression creep testing of weldments. M.S. Thesis T-2723, Colorado School of Mines, Golden, Colo.

18. Chu, S. N. G., and Li, J. C. M. 1980. Photoelastic studies of three-dimensional stress field caused by a cylindrical punch. *J. Appl. Phys.* 51 (6): 3338.

19. Gibbs, W. S., Wang, S. H., Matlock, D. K., and Olson, D. L. 1985. High-temperature impression creep testing of weldments. *Welding Journal* 64 (6): 153-s.

20. Wang, S. H., Matlock, D. K., and Olson, D. L. 1986. Unpublished research. Colorado School of Mines, Golden, Colo.

21. Sherby, O. D., and Burke, P. M. 1967. Mechanical behavior of crystalline solids at elevated temperature. *Progress in Materials Science 13* (7): 325.

22. Lisin, M. A. 1989. Impression creep testing within a microstructural gradient. M.S. Thesis T-3687, Colorado School of Mines, Golden, Colo.

23. Barrett, C. R., and Sherby, O.D. 1964. Steady-state creep characteristics of polycrystalline copper in the temperature range 400° to 950°C. *Trans. AIME* 230: 1322.

24. Evans, H. E., and Knowles, G. 1980. Dislocation creep in nickel and copper. *Metal Science* 14: 152.

25. Parker, J. D., and Wilshire, 8. 1978. Friction stress measurements during high-temperature creep of polycrystalline copper. *Metal Science* 12: 453.

26. Ashby, M. F. 1972. A first report on deformation mechanism maps. *Acta. Met.* 20: 887.

27. Monma, K., Suto, H., and Oikawa, H. 1964. High-temperature creep of nickel-copper alloys. *J. Japan Inst. Metals* 28: 258.

28. Nelmes, G., and Wilshire, B. 1976. Some factors affecting the creep resistance of single-phase copper alloys. *Scripta Met.* 10 (8): 697.

29. Bonesteel, R. M., and Sherby, O.D. 1966. Influence of diffusivity, elastic modulus, and stacking fault energy on the high-temperature creep behavior of the alpha brasses. *Acta Met.* 14: 385.

30. Correa da Silva, L. C., and Mehl, R. F. 1955. Interface and marker movements in diffusion of solid solutions of metals. *Trans. AIME* 191: 155.

31. Feltham, P., and Copely, G. J. 1958. Grain growth in alpha brasses. *Acta. Met.* 6: 539.

32. Evans, W. J., and Wilshire, 8. 1974. Sigmoidal transient creep behavior of 70-30 alpha brasses. *Scripta met.* 8 (5): 497.

33. Brandes, E. A., Ed. 1983. *Smithels Metals Reference Book,* 6th Ed., Butterworths, London, England, pp. 13-43.